JNC TN9400 2003-039

Improvement of SIMMER-Ⅲ Freezing Model

- A Study on a Semi-empirical Correlation for the Supercooling Temperature at the Melt/Structure Interface -

(Research Document)

June, 2003

O-arai Engineering Center

Japan Nuclear Cycle Development Institute

JNC TN9400 2003-039
June, 2003

Improvement of SIMMER-III Freezing Model

- A Study on a Semi-empirical Correlation for the Supercooling Temperature at the Melt/Structure Interface -

(Research Document)

Kenji Kamiyama*

Abstract

The SIMMER-III code has been developed to evaluate the sequences of core disruptive accidents (CDAs) in fast reactors (FRs). In order to reasonably evaluate the mass of molten fuel remained in the core region and the consequence of re-criticality, it is important especially for the code to evaluate phenomena adequately such as ejection, freezing and blockage formation inside the escape path.

The freezing model for the molten fuel has been developed and improved through the SIMMER-III phase 1 and 2 assessment programs. Especially, in the phase 2 assessments, knowledge of the metallurgy area was introduced, and it was found that a molten material formed the supercooling layer in the vicinity of structure wall and that the temperature of this layer dominated the energy loss of molten material and eventually the mass ejected into flow channel. This supercooling temperature was determined for each material based on the experimental result respectively as a constant input variable. On the other hand, experimental data used for the assessments of freezing model did not cover the temperature condition of CDA completely.

In this study, a semi-empirical correlation which is comprised of thermophysical properties is proposed to predict supercooling temperatures, in order to increase reliability and accuracy of SIMMER-III freezing model. To attain the generality of this semi-empirical correlation, not only the experimental data with molten uranium dioxide but also the data with tin and wood's metal were used in the derivation of this correlation, which have different thermophysical properties and temperature conditions. In addition, it was confirmed through the evaluation of experimental data that this correlation could be applied to the molten stainless steel freezing phenomena.

* FBR Cycle Safety Engineering Group, System Engineering Division, O-arai Engineering Center, JNC

JNC TN9400 2003-039
2003年6月

SIMMER-III 固化モデルの改良

—融体と構造材の接触境界面における過冷却温度に関する半実験式の検討—

（研究報告）

神山　健司*

要旨

SIMMER-III コードは、高速増殖炉の炉心崩落事故時（CDA）における事象進展を評価するため開発が進められてきた。特に、コードが溶融した燃料が分散経路に流出、固化・閉塞を生じる現象を適切に評価できることは、炉心内に残存する燃料量と再臨界の影響を合理的に把握することに繋がるため重要である。

溶融燃料の固化モデルは SIMMER-III コードの第1、2期検証研究を通じて改良されてきた。特に、第2期検証研究では冶金学の知見を取り入れ、融体と構造材の接触境界面に過冷却層が形成されること、この温度が融体の熱損失率を支配し融体分散量を定めることを見出した。この過冷却温度は、試験評価結果に基づいて物質毎に定め、入力にて一定値を与えていた。一方で、モデルの検証に用いた試験条件では、融体や構造材温度条件の点で実機 CDA の想定範囲を十分に含んではいない。

本研究では、固化モデルの信頼性および精度を高めるため、過冷却度を熱物性値にて予測できる半実験相関式を作成した。この相関式に一般性を持たせるため、二酸化ウランのみならず、異なる種類、温度条件を持つ錫および低融点合金の試験評価値も含めた。さらに、試験結果の評価により、この相関式は溶融ステンレス・スティールの固化挙動に対しても適用できることを確認した。

* 大洗工学センター　システム技術開発部　FBR サイクル安全設計グループ

Contents

List of Tables

List of Figures

Nomenclature

T : Temperature [K]
h : Heat transfer coefficient [W/m²/K]
q : Heat transfer rate [W/m³]
a : Interface area per unit volume [1/m]
Γ : Mass-transfer per unit volume [kg/s/m3]
i : Specific enthalpy [J/kg]
e : Specific internal energy [J/kg]
$\overline{\rho}$: Macroscopic density [kg/m³]
Δt : Time step [s]
κ : Thermal Conductivity [W/m/K]
D_h : Hydraulic diameter [m]
Nu : Nusselt number
Re : Reynolds number
Pr : Prandtl number
ρ : Density [kg/m³]
c_p : Heat capacity at constant pressures [J/kg/k]
Δ_s : Thickness of the steel can-wall surface node [m] (Normally, it is set about 0.3mm)
V_L : Velocity of fluid [m/s]
T_{scl}^I : Temperature of the supercooling layer [K]
Δ_c : Thickness of the crust [m]
L_p : Penetration length of molten material [m]
L_f : Latent heat of fusion [J/kg]
A : A factor of semi- empirical correlation determined by fitting of experimental data
π : A multiplier of semi- empirical correlation determined by fitting of experimental data

Subscripts

L : Liquid Phase Material
$L1$: Molten fuel
$L4$: Solid fuel particles
$L0$: Initial temperature of fluid
s : Structure
c : Crust
liq : Liquidus point
sol : Solidus point
I : Interface
L/s : Liquid-structure interface
n : Initial value
$n+1$: Updated value
IR : Interface resistance
scl : Supercooling layer

1. Introduction

One of the major concerns in the safety of fast reactors (FRs) is the possibility of re-criticality during so-called transition phase of postulated core disruptive accidents (CDAs). Although occurrence of CDAs is extremely unrealistic due to denying actuations of all the multiple safety systems, it still emphasized from the viewpoint of safety designs and evaluation. This is because it has potential that the molten fuel motion reaches the re-criticality configuration and releases energy to lose integrity of containment systems. This consequence of energetic re-criticality has been called "re-criticality issue" and is regarded as one of the most important risk contributors to the environments. The typical cause of reactivity insertion is a concentration of molten fuel due to two-dimensional oscillation during the core melting propagation. On the other hand, there are inherent mitigation mechanisms to decreases neutronic activity, in which pressure buildups during this propagation phase and molten fuel is ejected from the core region [1]. Therefore, it is quite important to evaluate adequately both these acceleration and mitigation mechanisms. For this purpose, the SIMMER-III code has been developed.

SIMMER-III is a two dimensional, three-velocity-field, multiphase, multicomponent, Eulerian, fluid-dynamics code coupled with a space- and energy-dependent neutron kinetics model. In order to provide SIMMER-III as a next-generation standard tool for FRs' safety analysis, assessment programs to study key accident phenomena were planned and have been performed in collaboration with European research institutes. Distribution and relocation of molten fuel is one of the key study areas in the assessment program. Especially, freezing of molten fuel and stainless steel on the core structure surface is a key phenomenon because the dynamics of freezing plays an important role in determining fuel removal from the core region. Thus, the freezing model in SIMMER-III has been developed and improved through the phase 1 and 2 assessment programs [2, 3]. As described in Chapter 2 in detail, the most important knowledge on the freezing phenomena is the formation of supercooling layer in the vicinity of the structure wall, and temperature of supercooling layer dominates the heat flux from a molten material to the structure wall. However, the experimental data used for the assessments of freezing model did not cover the temperature condition of CDA completely. Although the temperature of supercooling layer is material dependent value, it is given by an input constant based on experimental results.

Therefore, in order to improve SIMMER-III freezing model further, it is indispensable to predict the temperature of supercooling layer by theoretical or empirical correlations. The purpose of this study is to investigate the characteristics of

supercooling temperature and to try to derive an empirical correlation which is comprised of thermophysical properties to predict properly the supercooling temperature.

2. Experimental Knowledge on Freezing Phenomena and SIMMER-III Freezing Model

This chapter intends to clarify the relationship between the experimental knowledge and SIMMER-III freezing model. The following items are described in order: the basis for SIMMER-III freezing model at first, then experimental knowledge on freezing phenomena and their interpretations, and at last the improved model. Therefore, it is recommended to skip into Section 2.4.2 for whom intends to grab the gist of the improved SIMMER-III freezing model.

2.1. The Basis of SIMMER-III Freezing Model

Heat transfer between molten material and structures results in structure melting and/or freezing of molten materials (fuel and stainless steel). The first step calculates the phase transition process occurring at interface between molten material and structures, described by a non-equilibrium heat-transfer-limited model. The non-equilibrium process means that the bulk temperature does not generally satisfy the phase transition condition when the mass transfer occurs at the interface [4].

At the interface between molten materials and structures, the net energy transfer rate from the interface is described below:

$$q^I_{L/s} = a_{L/s} h_L \left(T^I - T_L\right) + a_{L/s} h_s \left(T^I - T_s\right) \tag{2-1}$$

If the value of equation (2-1) is zero, sensible heat is exchanged without phase transition at the interface.

If the value of equation (2-1) is negative, namely the energy increases at the interface, the structure melts, and the mass transfer rate is determined from:

$$\Gamma^I_{s,L} = \frac{q^I_{L/s}}{i_{liq,s} - i_s} \tag{2-2}$$

If the value of equation (2-1) is positive, namely the energy decreases at the interface, the molten material freezes. Then the mass transfer rate for this case is determined from:

$$\Gamma^I_{L,s} = \frac{q^I_{L/s}}{i_L - i_{sol,L}} \tag{2-3}$$

Here, the basic freezing modes are explained to help understanding on the relation

between freezing modes and SIMMER-III model. As shown in Fig. 2-1 , two concepts of blockage mode had been presented by the middle of 1980s. One is so-called "Conduction-limited freezing", in which the crust on the inner surface of flow channel grows to fulfill the flow area. The other is "Bulk freezing", in which the bulk enthalpy of flowing melt decreases and forms blockage by losing latent heat of fusion at the leading edge [Ref. 5, for example].

SIMMER-III code can simulate the conduction-limited freezing phenomena by setting the mass transfer rate of equation (2-3) into the crust. On the other hand, the bulk freezing phenomena is simulated in the equilibrium mass transfer process. This equilibrium process occurs when the bulk energy of molten material is reduced less than the liquidus energy as a result of heat loss. The energy loss was determined by:

$$\frac{\partial \overline{\rho}_L e_L}{\partial t} = \Gamma^I_{c,L} e_{Liq} - \Gamma^I_{L,c} e_L + a_{L/s} h_L \left(T^I - T_L\right) . \tag{2-4}$$

Here, for the simple explanation, the above equation expresses only one heat transfer pass between molten fuel and the structure wall.

The liquid freezes into solid particles, and the mass transfer rate is determined from:

$$\Gamma^{EQ}_{L1,L4} = \frac{\overline{\rho}_{L1}}{\Delta t} \frac{e_{Liq} - \widetilde{e}^n_{L1}}{e_{Liq} - e_{aol}}, \text{ where } e_{Liq} > e_{L1}, \text{ and} \tag{2-5}$$

$$\frac{\widetilde{\overline{\rho}}^{n+1}_{L4} - \widetilde{\overline{\rho}}^n_{L4}}{\Delta t} = \Gamma^{EQ}_{L1,L4} . \tag{2-6}$$

Generated solid particles are mixed with fluid and the effective viscosity of fluid increases slightly. Blockage of bulk freezing is simulated by increasing effective viscosity sharply when the fraction of solid particles in the fluid exceeds about 60%.

Heat transfer coefficients of the molten materials side are given by the following general empirical correlation:

$$h_L = \frac{\kappa_L}{D_h} Nu, \quad \text{where} \quad Nu = 0.023\,\mathrm{Re}^{0.8}\,\mathrm{Pr}^{0.3} \quad \text{for the molten fuel and}$$

$$Nu = 5 + 0.025\,\mathrm{Re}^{0.8}\,\mathrm{Pr}^{0.8} \quad \text{for the molten steel.} \tag{2-7}$$

Heat transfer coefficients of the structure side are simply given by

$$h_s = \frac{2\kappa_s}{\Delta_s} \quad . \tag{2-8}$$

Interface temperature between the molten fuel and steel structures are defined by the following equation which is derived from instantaneous contact temperature of two semi-infinite bodies:

$$T^I = \frac{\sqrt{(\rho c_p \kappa)_L}\, T_L + \sqrt{(\rho c_p \kappa)_s}\, T_s}{\sqrt{(\rho c_p \kappa)_L} + \sqrt{(\rho c_p \kappa)_s}} \quad . \tag{2-9}$$

For the crust surface, the interface temperature is defined by the solidus temperature of the crust.

Interface temperature when the liquid steel is in contact with steel structures is defined by the following:

$$T^I_{steel} = \min\left[T_{Liq,steel}, \max\left(\frac{h_L T_L + h_s T_s}{h_L + h_s}, T_{sol} \right) \right] \quad . \tag{2-10}$$

2.2. Experimental Knowledge on Freezing Phenomena

Studies of freezing phenomena closely related to FRs' safety have been started since 1970s in which a various simulant (water, Freon, etc.) and molten fuel were used. By the middle of 1980s, supposing the conduction limited freezing or bulk freezing, theoretical models and experimental correlations were presented. These studies were conducted mainly by Argonne National Laboratory in the United States. Basis for SIMMER-III freezing model described in Section 2.1 is based on the above knowledge. On the other hand, modification of freezing model which is described later in Section 2.4 is based on studies in the late 1980s in which knowledge from metallography and metallurgy areas were introduced.

First of all, fundamental knowledge on the relation between crystal types and their formation process are remarked because they are important for the further discussion. Figure 2-2 illustrates the solidification process in a metal casing. Three different varieties of grain types are observed, and their formation processes can be explained below by considering descriptions in references 6 and 7.

- Firstly, in the vicinity of the mold wall, where the cooling rate is highest, solid nuclei appear, grow-up to crystals and they form so-called equiaxed chill zone

(or chill zone simply). It is necessary for solid nuclei appearance to go through the supercooling process, in which liquid is cooled below its solidus temperature. In this report, the (equiaxed) chill zone is used interchangeably with the supercooling layer.

- Next, crystals grow parallel and opposite to heat flow direction, leading to formation of columnar zone.

- At last, equiaxed zone is formed inside the columnar zone. Interpretations of this equiaxed zone differ as to researchers. The major interpretation is that branches of columnar structure are detached and grow-up to equiaxed crystal. Another major interpretation is that solid nuclei are detached from the mould wall or surface, transferred inward by convection before the columnar structure is formed, and grow up to equiaxed crystals The latter seems to be likely judging from some experiments described in the reference 6.

In the experiment described in the reference 8, based on the analysis of experiments in which pure molten tin was injected into tubular Pyrex molds [9], crystal distributions along the flow direction are divided into four regions as illustrated in Fig. 2-3.

- Region A: Near the mold entrance, a small number of large crystals grow parallel to the mold wall.

- Region B: Columnar crystals grow inward from the mold wall. A small number of equiaxed crystals exist at the center part.

- Region C: Equiaxed crystals in the central region gradually increase comparing with columnar crystals on the wall.

- Region D: Only small size of equiaxed crystals exist.

The post-test examinations of selected the experiment from Geyser program, in which molten uranium dioxide at 3000 deg.-C was injected into the steel tube with 4mm inner diameter at room temperature, indicates the followings [10]:

- At the position 24cm from the inlet, the solidified uranium dioxide exhibits a typical columnar structure with the chill zone at the wall surface. The width of columnar structure is 400 micrometer and of chill zone is 50 micrometer.

- At the position 44cm from the inlet, the solidified uranium dioxide is formed by equiaxed crystals.

Geyser experiment was performed by Commissariat à l'Energie Atomique (CEA), France,

and the above observation was result from No.1 test in which the molten uranium dioxide penetrated and formed the blockage at 65cm from the inlet.

In addition, the microstructure observation in the reference 11 shows the contact resistance between the molten fuel and steel structure due to wettability.

2.3. Interpretations of Experimental Knowledge

One can deduce from Fig. 2-2 and Fig. 2-3 that the so-called crust is columnar crystals and the plugging of bulk freezing is formed by equiaxed crystals, and that the crystal distributions of solidified uranium dioxide in Geyser experiment are consistent with Fig. 2-3. In other words, the microstructure analysis of solidified uranium dioxide reveals the crust formation on the wall upstream region and formation of bulk-type plug at the leading edge.

From the experimental knowledge described in Section 2.2, the freezing process of flowing molten material inside the tube can be explained as follows [12]. This explanation is presented in Fig. 2-4.

- The molten material makes contact with the steel wall at discrete points, and is cooled by heat conduction through contact points. During this cooling process, the molten material at the vicinity of the wall interface is cooled below its solidus temperature.

- During this supercooling process, solid nuclei appear and grow-up to crystals, and they form equiaxed chill zone. When solid nuclei appear, the supercooling region is heated up because latent heat of fusion is released. In other words, the level of supercooling is limited by nucleation.

- Crystals in the chill zone grow parallel and opposite to heat flow direction, leading to formation of columnar zone. The gap is formed between the crust and a steel wall due to discrete contact between the molten material and a steel wall.

- The bulk enthalpy of flowing melt decreases and the plugging is formed by equiaxed crystals.

For the present, it may be useful to discuss the process of plugging formation depending on the fact that solidified material at the leading edge is formed by equiaxed crystals. It is described in reference 6 that four conditions are necessary to make a large percentage of solidified phases from equiaxed crystals. For the flowing melt

inside tube, the following three conditions are important:

- To prevent stable solid shell formation.
- To promote release of crystal formed at vicinity of the wall.
- To prevent released crystals from re-melting.

The first condition is satisfied because the discrete contact to the wall limits the nucleation density. In order to satisfy the second condition, crystals formed in the vicinity of wall should be entrained into the flow, so that it is reasonable to suppose turbulent flow until the plugging formation. In addition, the bulk temperature of the melt should be reduced to liquidus point to satisfy the third condition. It should be noted that the bulk temperature is hard to be cooled below its solidus temperature under the disturbance condition like turbulent flow. In contrast, liquid near the wall surface can be supercooled because the viscous sublayer is formed here.

Thus, one can explain the fact that solidified material at the leading edge is formed by equiaxed crystals as follows:

- Crystals are formed in the supercooling layer in the vicinity of the wall, transferred by convection and mixed with the mainstream of melt which loses sensible heat.
- Through this process, the solid fraction increases and at last the plugging is formed.

Thus, it is reasonable to consider that the flow state is turbulence just before the plugging formation. This suggests that effective viscosity cannot increase significantly after loss of sensible heat. In this point, the basic concept of current SIMMER-III model for blockage formation, briefly described in Section 2.1, is reasonable for freezing of flowing melt.

2.4. Improvements of SIMMER-III Freezing Model

2.4.1. Improvements in the Phase 1 Code Assessment

Validation of freezing model was started from the phase 1 code assessment program [2]. Two types of experimental data, one is conduction-limited freezing [13] and the other is bulk freezing [11], are used to assess the model. This assessment showed that SIMMER-III freezing model described in Section 2.1 successfully reproduced experimental results in which molten alumina was injected into a cold tube and the blockage was formed by conduction limited freezing. On the other hand, as the circles

of Fig. 2-5, SIMMER-III bulk freezing model significantly underestimate the experimental results, in which molten fuel was injected into the cold steel channel.

For the model improvement, interfacial contact resistance between molten material and a steel wall was introduced based on experimental evidence in reference 11. The concept of this interface resistance is shown in Fig. 2-6. In this improved model, the overall heat transfer coefficient including the contact resistance between the fluid and the structure is given by experimental result. That is,

$$h_{GB} = 800 \frac{\kappa_L \kappa_s}{\kappa_L + \kappa_s} V_L \ , \tag{2-11}$$

where,

$$\frac{1}{h_{GB}} = \frac{1}{h_L} + \frac{1}{h_{IR}} + \frac{1}{h_s} \ . \tag{2-12}$$

Here, h_{IR} means the heat transfer coefficient to express the contact resistance due to discrete contact between the molten materials and the structure. Heat transfer coefficients of h_L and h_s are given by equations (2-7) and (2-8). In addition, supposing that non-equilibrium phase change dose not occur, the following heat flux conservation is given:

$$h_L\left(T_L - T_L^I\right) = h_{IR}\left(T_L^I - T_s^I\right) = h_s\left(T_s^I - T_s\right) \ . \tag{2-13}$$

In this way, interface temperatures are determined, and thus heat loss rate can be evaluated.

The introduction of interface resistance model significantly improved the prediction of molten fuel penetration lengths as shown by the squares in Fig. 2-5.

2.4.2. Improvements in the Phase 2 Code Assessment

Improved freezing model in the phase 1 assessment study dose not take all of experimental knowledge described in Section 2.2 into account. It introduced only the contact resistance, so that there were rooms for further improvements. Therefore, continuous improvement on SIMMER-III freezing model was carried out to introduce interpretations of experimental knowledge described in Section 2.3 [3, 12].

When one focuses attention to the supercooling at the interface between the fluid and the structure, it is ideal to divide fluid and structure into fine mesh cells and to

simulate supercooling and latent heat release process in detail. However, it requires code restructuring, and therefore the model improvement was performed within code limitations, which is one temperature point for the fluid, one interface temperature and two temperature points for the steel can-wall structure. A brief overview of the improved model is explained below.

Heat transfer coefficient for the element i through discrete contact points is given by:

$$h_{IR,i} = \frac{4\xi\kappa_l\sqrt{N}}{g(\xi)\sqrt{\pi}} \quad , \tag{2-14}$$

where, ξ is the ratio of contact length to separation length, and 0.1 is assigned based on microstructure analysis. A function $g(\xi)$ is defined by

$$g(\xi) = 1 - 1.40925\xi + 0.40925\xi^3 \tag{2-15}$$

Contact density N is given by

$$N = C_{p1} + C_{p2}V_L^2 \quad , \tag{2-16}$$

to which, $C_{p1} = 40\times10^6$ and $C_{p2} = 2.5\times10^6$ give the best agreement with experimental results.

For the non-equilibrium processes, the following criterion is introduced. For the non-equilibrium melting of the steel structures, it is given by:

$$h_L\left(T_l - T_{scl}^I\right) \geq \mathrm{h_{s,IR}}\left(T_{s,sol} - T_s\right), \text{ where } h_{s,IR} = \frac{4\kappa_s\xi\sqrt{N}}{g(\xi)\sqrt{\pi}} \quad . \tag{2-17}$$

This criterion simply means that the energy transferred from flowing molten material to supercooling layer exceeds the energy which can be extracted by the steel wall without melting of the wall surface.

On the other hand, non-equilibrium freezing of molten material occurs when the energy extracted through the supercooling layer exceeds the energy transferred from flowing molten material to supercooling layer. This is given by:

$$h_{IR,sum}\left(T_{scl}^I - T_s\right) \geq h_L\left(T_L - T_{scl}^I\right) \quad , \tag{2-18}$$

where

$$h_{IR,sum} = \left(\frac{1}{h_{IR,scl}} + \frac{1}{h_{IR,s}} + \frac{1}{h_s} \right)^{-1} \text{, and } h_{IR,scl} = \frac{4\xi\kappa_L\sqrt{N}}{g(\xi)\sqrt{\pi}} \quad . \tag{2-19}$$

If neither equations (2-18) nor (2-19) are satisfied, non-equilibrium mass transfer dose not occur.

It is noted that T_{scl}^{I} is temperature of the supercooling layer and is used as an interface temperature between molten materials and steel structures instead of temperature defined by equation (2-9). The rate of bulk enthalpy loss for molten materials is controlled by this temperature as shown in the equation (2-4). As for freezing of molten uranium dioxide, by assuming that temperature of supercooling layer is 2940K, SIMMER-III evaluation gives the best agreement with experimental results as shown by diamond marks in Fig. 2-7. Here, it should be commented that experimental data used molten thermite, which is mixture of uranium dioxide and molybdenum, were excluded from the phase 2 assessment study due to uncertainty of its thermophysical properties. Therefore, some experimental data plotted in Fig. 2-5 are excluded from Fig. 2-7.

Experimentally observation of crust formation is that solid nuclei appear, grow-up to crystals to form so-called chill zone and crystals grow parallel and opposite to heat flow direction, leading to formation of columnar zone. Therefore, SIMMER-III code recognizes a crust formation when thickness of a solidified layer exceeds that of chill zone. This criterion is simply defined by

$$\Delta_c > \Delta_{scl} = W_{crust} \times b \quad , \tag{2-20}$$

where, $W_{crust} = 0.5$ is consistent with the experimental result, and

$$b = \sqrt{\frac{1}{\pi N}} \quad . \tag{2-21}$$

When the crust forms, the contact resistance exists between the crust and a steel wall due to discrete contact between the molten material and steel wall. Thus, the overall heat transfer coefficient between the crust and a steel wall is determined by:

$$h_{IR,sum} = \left(\frac{1}{h_c} + \frac{1}{h_{IR,scl}} + \frac{1}{h_{IR,s}} + \frac{1}{h_s} \right)^{-1} \text{, where } h_c = \frac{2\kappa_c}{\Delta_c} \quad . \tag{2-22}$$

The generality of the improved freezing model was assessed by SIMMER-III applications to the freezing experiments in which simulant, molten tin and wood's metal, were injected into and frozen inside a steel tube [14, 15]. In this application, only the temperatures of supercooling layer were varied as follows, taking the difference of solidus and liquids temperatures into account:

- For tin, $T_{scl}^{I} = 450K$ (55K supercooling).
- For Wood's Metal, $T_{scl}^{I} = 365K$ (32K supercooling).

Results of SIMMER-III evaluation are given by square and circle dots in Fig. 2-7 [3]. One can deduce from this figure that SIMMER-III improved freezing model can be validated because it reasonably reproduces experimental results with different thermophysical properties and temperature condition.

Studies in the phase 2 assessment reveal that all of the experimental results can be explained using a constant supercooling temperature depending on each molten material, although this temperature varies through the successive processes of supercooling by conduction in the vicinity of a wall, nucleation and heating by latent heat release. Therefore, from the practical standpoint, it is quite reasonable to define the supercooling temperature slightly heated by latent heat release at the time scale when the convection heat transfer is evaluated using the empirical heat transfer correlation.

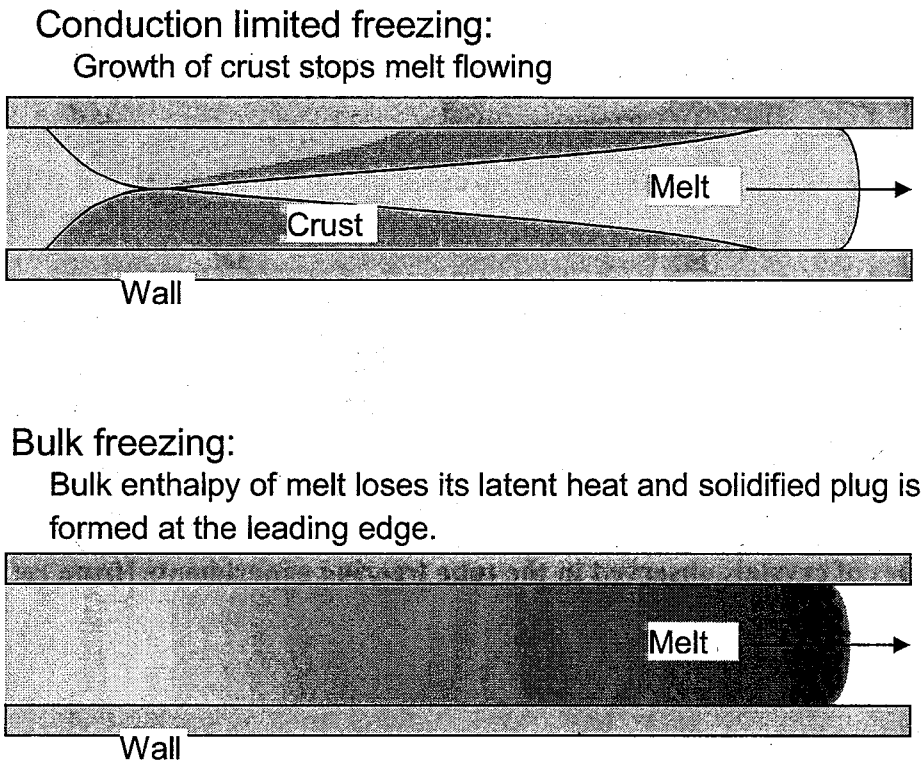

Fig. 2-1 Two classical concepts of blockage mode

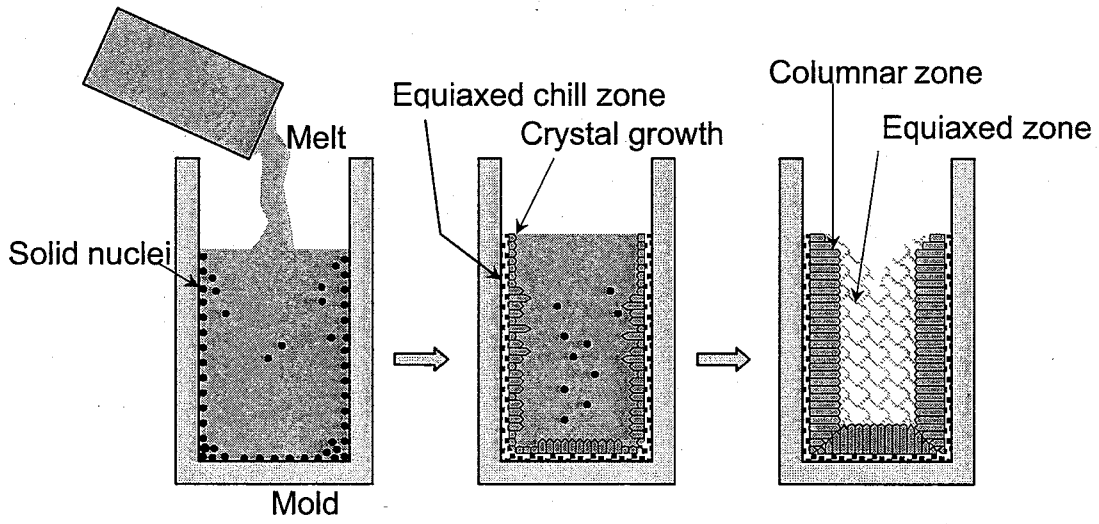

Fig. 2-2 Solidification process and types of crystals formed in casting

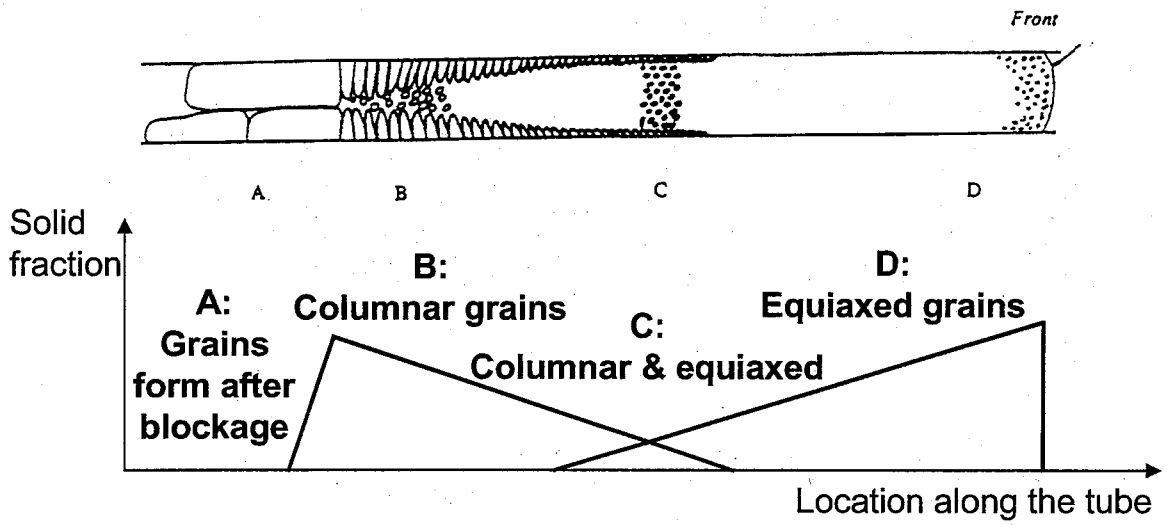

Fig. 2-3 Types of crystals observed in the tube freezing experiments [from ref. 8]

(a) Freezing process at a point on the surface

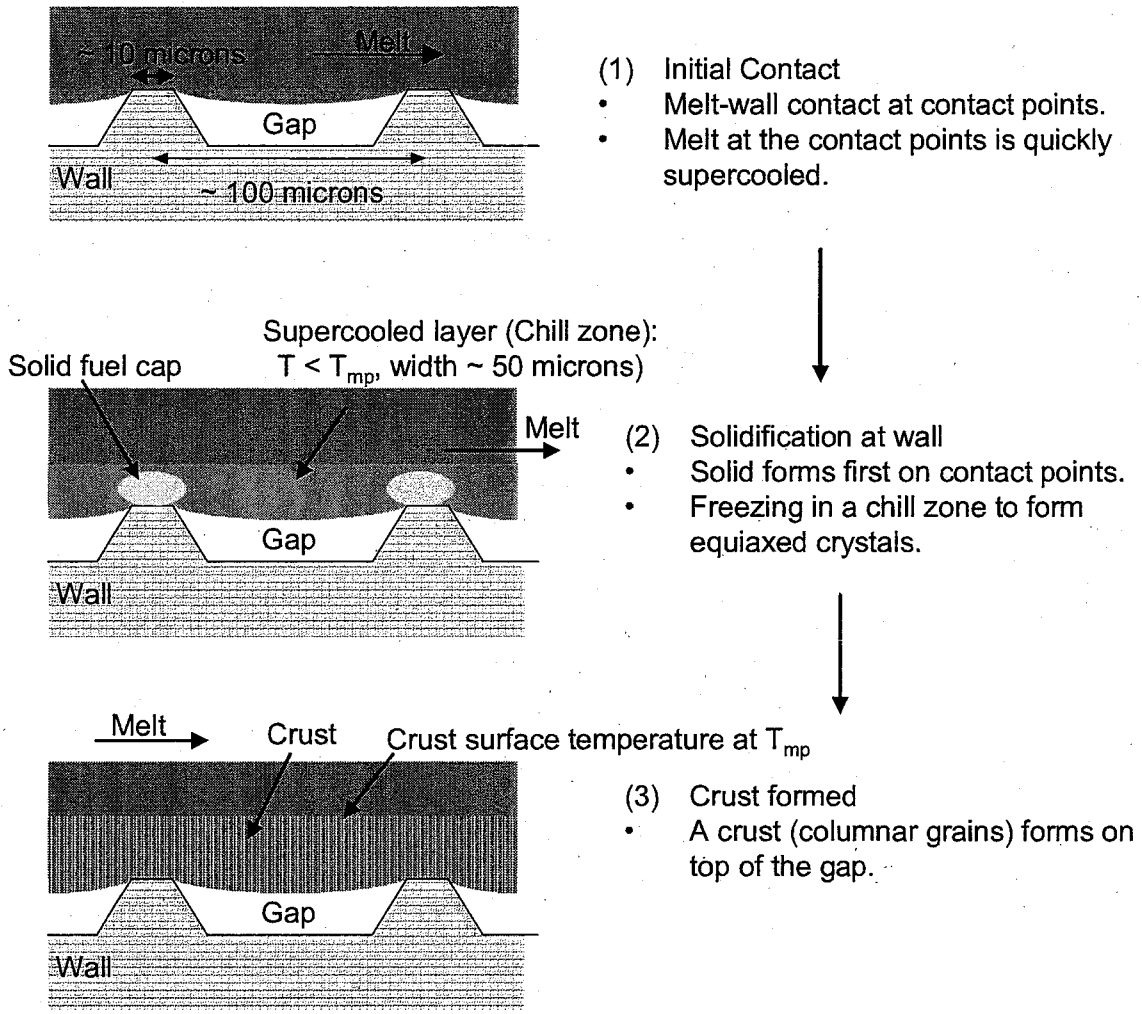

(b) Freezing process at a point in time

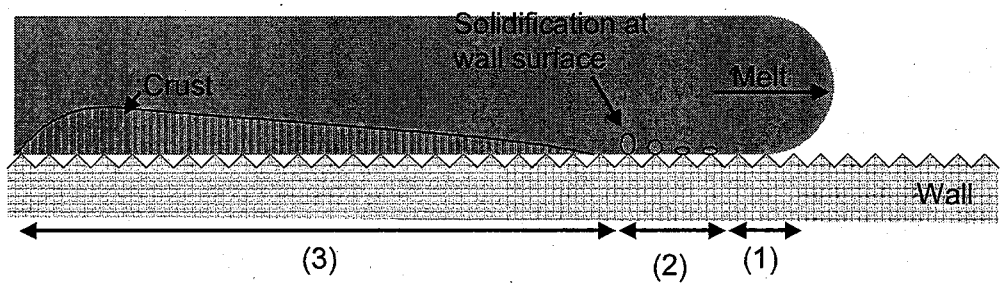

Fig. 2-4 Schematic representation of freezing process in the flowing melt [12]

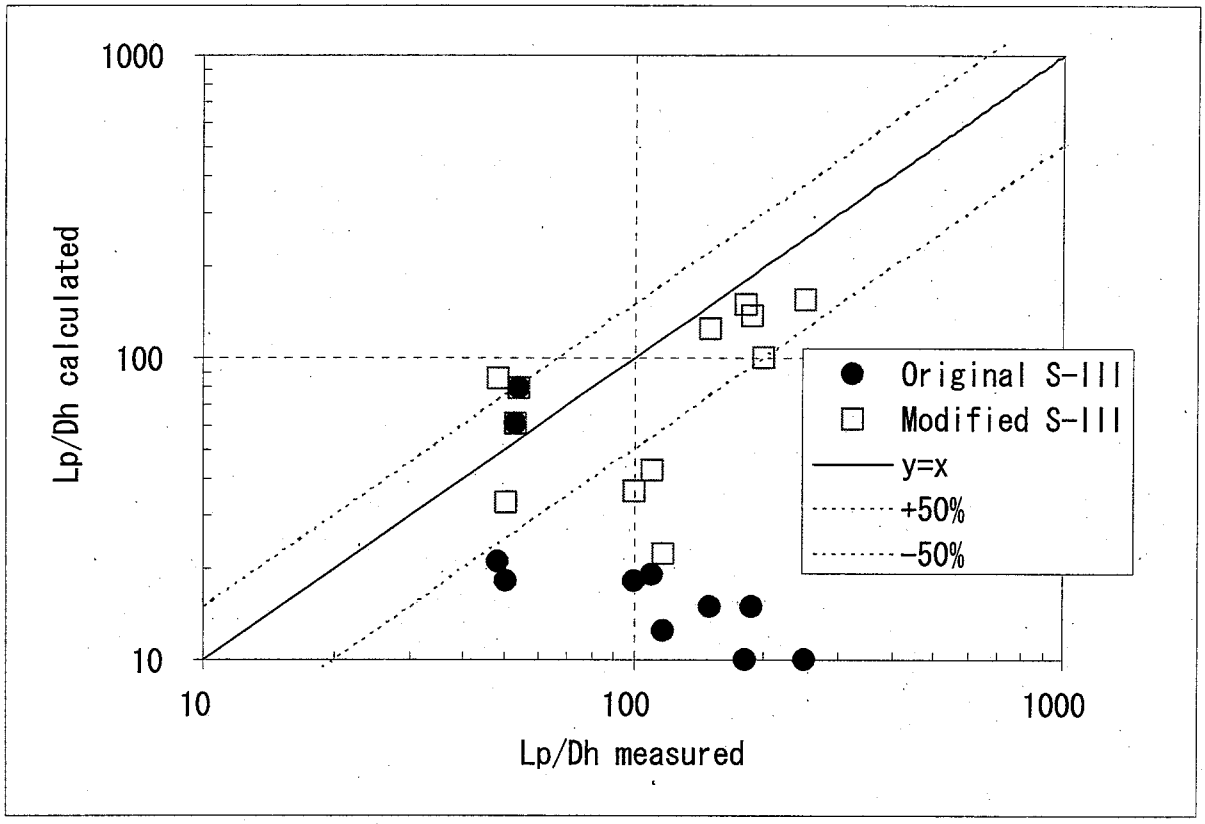

Fig. 2-5 SIMMER-III evaluation of bulk freezing model in the phase 1 code assessment study [From ref. 2・

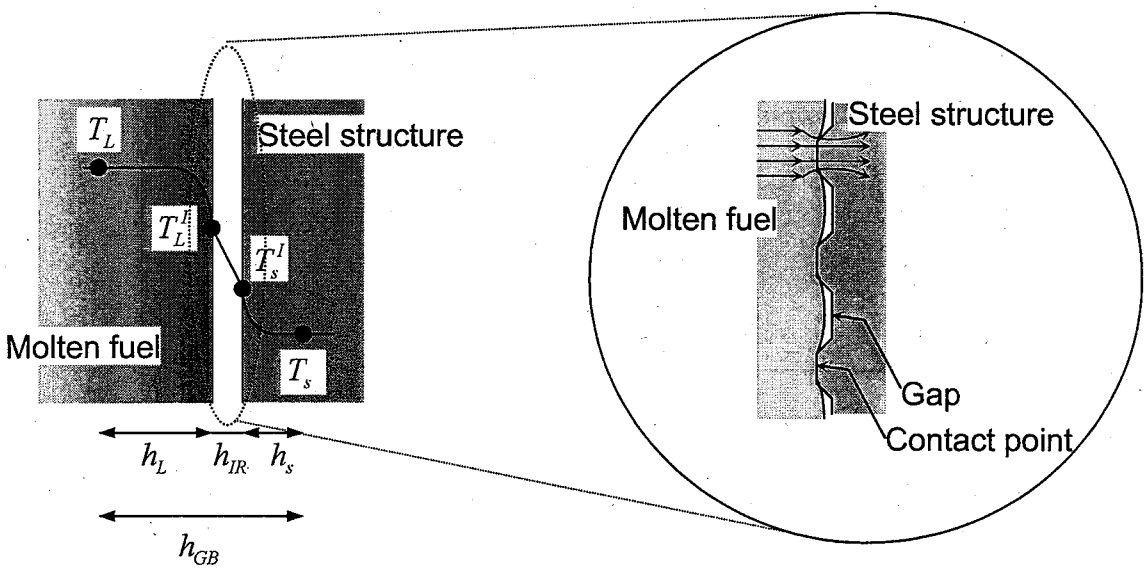

Fig. 2-6 The schematic representation of the interface resistance model

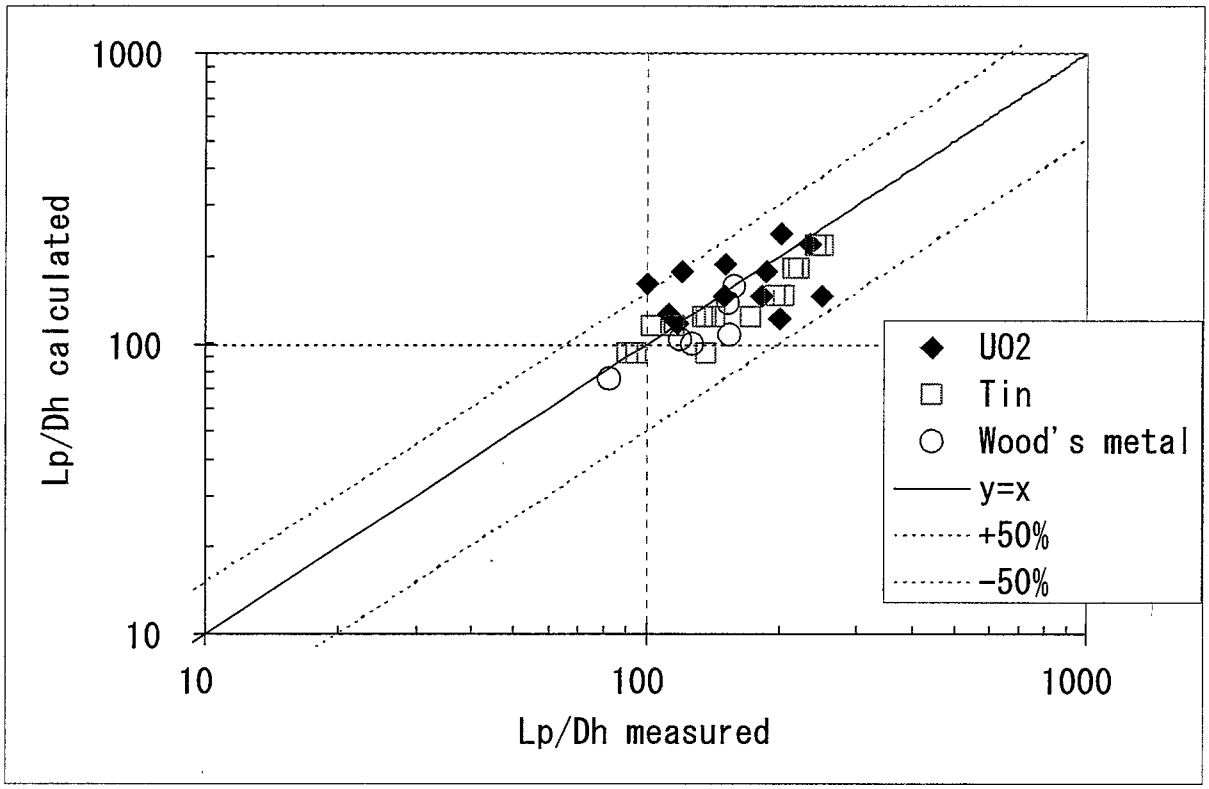

Fig. 2-7 SIMMER-III evaluation of improved bulk freezing model in the phase 2 code assessment study [from ref. 3]

3. Derivation of Semi-empirical Correlation for Supercooling Temperature Prediction

As discussed in Chapter 2, the supercooling layer is formed in the vicinity of a wall surface, and its temperature dominates the rate of bulk enthalpy loss, so that it is quite important for the freezing evaluation to determine temperature of the supercooling layer. However, since the supercooling process for flowing molten materials is too rapid to measure, temperature of the supercooling layer is evaluated indirectly based on initial condition and results of experiments. This temperature is determined for each molten material. For molten uranium dioxide, 2940K is used and is given by input constant in SIMMER-III. However, in order to increase reliability and accuracy of SIMMER-III freezing model, it is indispensable to define the supercooling temperature by theoretical or semi-empirical correlation, since the experimental conditions so far not necessarily cover the whole CDA condition

In this chapter, we try to derivate the semi-empirical correlation and introduce it into SIMMER-III.

3.1. Discussion on Supercooling Temperature and Derivation of Semi-empirical Correlation

In the following discussion, to prevent the confusion of terms, the term "supercooling temperature" is used to refer to the temperature difference between liquidus temperature and temperature of the supercooling layer, and this term is strictly distinguished from the term "temperature of the supercooling layer". As mentioned in Section 2.4.2, the evaluated "temperatures of supercooling layer" for molten uranium dioxide, tin and wood's metal are 2940, 450 and 365K respectively. Thus, "supercooling temperatures" for uranium dioxide, tin and wood's metal become 180K ($T_{liq} = 3120K$), 55K ($T_{liq} = 505K$) and 32K ($T_{liq} = 397K$) respectively.

First of all, the relation between the evaluated supercooling temperature and their liquidus temperature is plotted in Fig. 3-1. This figure shows the tendency that the molten material with higher liquidus temperature has the higher supercooling temperature. This tendency agrees with Fig. 3-2 which shows the relation between supercooling temperatures of pure metal and their liquidus points [6]. It is clear that the liquidus temperature is the important property and should be taken into account in the semi-empirical correlation. Here, it should be noted the difference of supercooling temperatures shown in Fig. 3-1 and Fig. 3-2. The former represents the temperature in which the latent heat releases by nucleation are included as explained in Sections 2.2 and 2.4.2. On the other hand, the latter(Fig. 3-2) is obtained by cooling the bulk liquid

carefully to avoid nucleation. Therefore, the supercooling temperatures in Fig. 3-1 become smaller than these of Fig. 3-2.

Here, we put a simple assumption that, in addition to the liquidus point of molten material, the conduction cooling by the wall and thermophysical properties also dominates the supercooling temperatures, because the molten material is cooled by conduction at the start of contact and thermophysical properties have effects on the contact temperature. Therefore, the following function is assumed:

$$\frac{\Delta T_{sc}}{\Delta T_{con}} = A\beta^{\pi 1}\left(\frac{T_{liq}}{\Delta T_{con}}\right)^{\pi 2} \quad \text{, where } \beta = \left(\rho c_p \kappa\right)_L / \left(\rho c_p \kappa\right)_s \quad . \tag{3-1}$$

In order to determine the factor A and multipliers $\pi 1$ and $\pi 2$ by fitting the experimentally evaluated supercooling temperatures, equation (3-1) is expressed by non-dimensional formula. Here, ΔT_{sc} means the supercooling temperature and ΔT_{con} is defined by

$$\Delta T_{con} = T_{liq} - T_{con}^{I} \quad , \tag{3-2}$$

where, T_{con}^{I} is temperature defined by the heat conduction.

Although, as described in Section 2.3, the molten material makes contact with a wall at discrete points, both molten material and a wall can be considered as semi-infinite at the start of contact. Therefore, T_{con}^{I} is defined here by:

$$T_{con}^{I} = \frac{\sqrt{\left(\rho c_p \kappa\right)_L}\, T_L + \sqrt{\left(\rho c_p \kappa\right)_s}\, T_s}{\sqrt{\left(\rho c_p \kappa\right)_L} + \sqrt{\left(\rho c_p \kappa\right)_s}} \quad . \tag{3-3}$$

Hence, equation (3-2) is expressed by:

$$\Delta T_{con} = T_{liq} - \frac{\sqrt{\left(\rho c_p \kappa\right)_L}\, T_L + \sqrt{\left(\rho c_p \kappa\right)_s}\, T_s}{\sqrt{\left(\rho c_p \kappa\right)_L} + \sqrt{\left(\rho c_p \kappa\right)_s}} \quad , \tag{3-4}$$

and finally experimental data of uranium dioxide, tin and wood's metal can be plotted in Fig. 3-3, where the vertical axis is given by the left part of equation (3-1) and horizontal axis by $\beta^{\pi 3}\left(T_{liq}/\Delta T_{con}\right)$.

Therefore, the formula of fitting function is expressed by:

$$y = Ax^{\pi 2} = A\left(\beta^{\pi 3}\frac{T_{liq}}{\Delta T_{con}}\right)^{\pi 2} \tag{3-5}$$

By altering the multiplier $\pi 3$ with trial and error, the following function is obtained which shows good agreement with experimental data:

$$y = 0.083x^{1.147} = 0.083\left(\beta^{0.240}\frac{T_{liq}}{\Delta T_{con}}\right)^{1.147} \tag{3-6}$$

This function is represented by the continuous line in Fig. 3-3.

Therefore, from the equations (3-1) and (3-6), the following function can be obtained:

$$\Delta T_{sc} = 0.083\beta^{0.275}T_{liq}^{1.147}\Delta T_{con}{}^{-0.147} \tag{3-7}$$

Eventually, the supercooling temperature can be evaluated by

$$\Delta T_{sc} = 0.083\beta^{0.275}T_{liq}^{1.147}\left(T_{liq} - \frac{\sqrt{\beta}T_L + T_s}{\sqrt{\beta}+1}\right)^{-0.147} \tag{3-8}$$

Thermophysical properties used in the discussion above are shown in Table 3-1. Properties for uranium dioxide and stainless steel are same as used in SIMMER-III.

3.2. Application of Semi-Empirical Correlation for Molten Stainless Steel

Molten stainless steel exists with molten fuel under CDA condition and its relocation behavior is considered to play an important role for CDA sequence, so that it is indispensable to evaluate the supercooling temperature of molten stainless steel adequately. The basis of semi-empirical correlation obtained in Section 3.1 does not include the experimental data of stainless steel due to very limited data base. However, it may be useful to validate the semi-empirical correlation using some available data. Thus, simple evaluation is performed for selected two experiments to investigate the fundamental applicability of the semi-empirical correlation to molten stainless steel.

The first data is Geyser No. 5 experiment which was conducted as a variation of Geyser series experiment [8]. The experimental condition and results are shown in Table 3-2. First of all, the supercooling temperature is evaluated by the semi-empirical correlation. There is a little temperature dependency, that is

$\Delta T_{sc} = 188K$, at $T_L = 2073K$ and $\Delta T_{sc} = 197K$, at $T_L = 1753K$.

Thermophysical properties used for this evaluation are shown in Table 3-3.

Supposing that the crust formation at leading edge of flowing melt can be negligible, the penetration length of melt is evaluated by the following equation which is based on the bulk freezing model:

$$L_p = \frac{\rho_L D_h V_L}{4h_L}\left[c_{p,L}\ln\left(1+\frac{T_{L0}-T_{liq}}{\Delta T_{sc}}\right)+\frac{fL_f}{\Delta T_{sc}}\right], \qquad (3\text{-}9)$$

where f means that the molten material stops flowing when it loses a certain portion $(f<1)$ of latent heat, and $f=0.6$ is used in the following evaluations so as to be consistent with the SIMMER-III model. The derivation of equation (3-8) is described in Appendix A.

Since the velocity of flowing melt was not measured in the Geyser 5 test, two calculations were performed varying velocities 3.0 and 4.0 m/s which are guessed from the another Geyser tests performed in the similar condition. The evaluated penetration lengths by equation (3-8) are 0.39 and 0.44m, which are 12-21% under estimation of the experimental result.

The second experimental data is that molten stainless steel is injected into alumina nozzle which was performed using MELT-II facility in O-arai Engineering Center, Japan Nuclear Cycle Development Institute. The summary of experimental condition and results are shown in Table 3-4, and details are described in Appendix B. The evaluated supercooling temperature is about 151K for the test SSFR-10-01 by the equation (3-7) using thermophysical properties shown in Table 3-3. The evaluated penetration length by equation (3-8) is 1.16m which 14-22% under estimation of the experimental result. For the test SSFR-30-01, the evaluated penetration length becomes 5.1m and it is consistent with the test result, which the molten stainless steel. did not form the blockage and flew out of the alumina nozzle of 2.15m.

From the evaluations shown above, it seems reasonable to conclude that the semi-empirical correlation (3-7) can basically apply the molten stainless steel because it can evaluate penetration lengths within error of 12-22%. Needless to say, experimental data concerning to molten stainless steel are required to further increase the quality and reliability of the current correlation.

3.3. Introduction into SIMMER-III

It is quite simple to introduce the semi-empirical correlation obtained in Section 3.1 into SIMMER-III. Instead of the input constant variable, the following equation provides the interface temperatures between molten fuel and steel structures, and between molten stainless steel and steel structures:

$$T_{scl}^{I} = T_{liq} - \Delta T_{sc} = T_{liq} - a_{sc}\beta^{\pi 1} T_{liq}^{\pi 2}\left(T_{liq} - \frac{\sqrt{\beta}T_L + T_s}{\sqrt{\beta}+1}\right)^{1-\pi 2} \qquad (3\text{-}10)$$

where, a_{ac}, $\pi 1$ and $\pi 2$ are given by input variables newly defined in SIMMER-III. Their names and default values are:

CASC= a_{ac} =0.083,

PSC1= $\pi 1$ =0.275, and

PSC2= $\pi 2$ =1.147.

It should be noted that the supercooling temperature can not exceed the conduction cooling temperature, so that the following condition should be satisfied:

$$\Delta T_{sc} < \Delta T_{con} \quad . \qquad (3\text{-}11)$$

If this condition is not satisfied, the supercooling temperature is given by:

$$\Delta T_{sc} = \Delta T_{con} \quad . \qquad (3\text{-}12)$$

In order to validate the introduced semi-empirical correlation, re-calculation of Geyser-4 test was performed. Figure 3-4 shows axial material distribution and a blockage is formed at 0.222 second. One can deduce from Fig. 3-4 that the final penetration length is 0.61m and agrees with the experimental result, 0.6m, and that the characteristics of solidified material distribution also shows a good agreement with the experimental observation shown in Fig. 2-3.

If a user wants to reduce the penetration length of molten materials, a lager value should be given to input variable CASC. However, one should notice that the default values are determined based on the experimental analysis, so that to change input variables CASC, PAC1 and PSC2 violates the basis of experimental knowledge.

Table 3-1 Thermophysical properties used for study on semi-empirical correlation

	Material		Density [kg/m^3]	Heat Capacity [J/kg/k]	Thermal conductivity [W/m/K]	Latent heat of fusion [J/kg]	Liquidus temperature [K]
Melt	UO_2		8860	520	3.15	2.77E+05	3120
	Wood's Metal		10500	150	11.1	2.53E+04	397
	Sn		6930	245	33.0	6.06E+04	505
Wall	Stainless steel	283~293K	7880	500	13.9	-----	-----
		673K	7770	610	19.4	-----	-----

Note: Variable of uranium dioxide and stainless steel are based on References 16, 17 and 18.

Table 3-2 Condition of GEYSER-Steel test and results

Test No.	Initial Condition				Result
	Inner Diameter [mm]	Tube temperature [deg. C]	Melt temperature [deg. C]	Driving pressure [bar]	Penetration length [cm]
5	4	20	1800	3	50

Table 3-3 Thermophysical properties used for evaluation of stainless steel freezing tests

	Material	Density [kg/m^3]	Heat Capacity [J/kg/k]	Thermal conductivity [W/m/K]	Latent heat of fusion [J/kg]]	Liquidus temperature [K]	Viscosity [Pa*s]
Melt	stainless steel	6900	700	17	3.39E+05	1753	0.0075 [at 1753K] 0.007 [at 1780K] 0.005 [at 2070K]
Wall	stainless steel	7880	500	13.9	---	---	---
	Al_2O_3	3890	779	36	---	---	---

Table 3-4 Summary of initial conditions and results for molten stainless steel ejection tests

Test No.	Initial Condition			Result	
	Inner diameter of nozzle [mm]	Nozzle temperature [deg. C]	Melt temperature [deg. C]	Average Velocity [m/s]	Penetration length [m]
SSFR-10-01	10	16 - 77.4	1506	3.45	1.35 - 1.49
SSFR-30-01	30	9.6 - 59.6	1532	3.97	Over 2.15

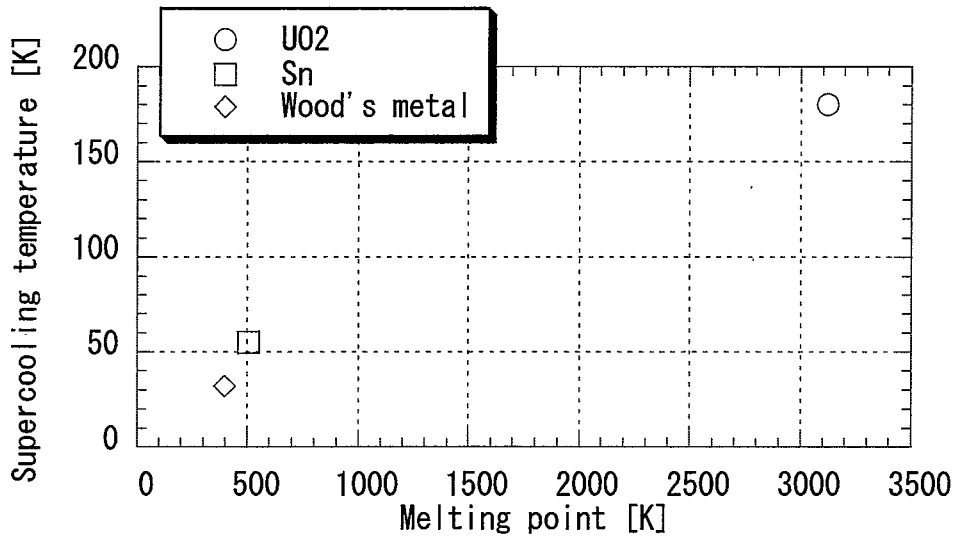

Fig. 3-1 Relation between the liquidus temperature and evaluated supercooling temperatures

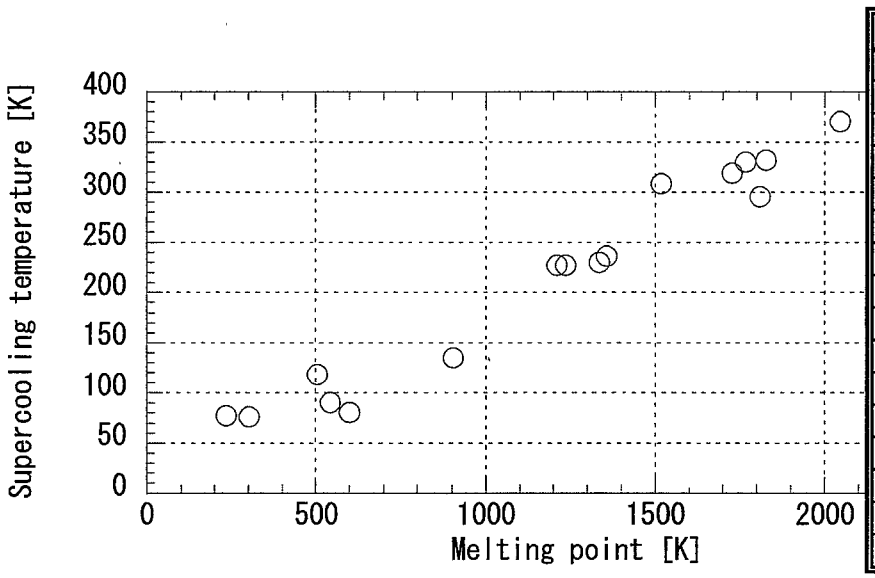

Material	X	Y
Hg	234	77
Ga	302	76
Sn	505	118
Bi	544	90
Pb	600	80
Sb	903	135
Ge	1210	227
Ag	1235	227
Au	1337	230
Cu	1357	236
Mn	1517	308
Ni	1728	319
Co	1767	330
Fe	1810	295
Pd	1827	332
Pt	2045	370

Fig. 3-2 Relation between the liquidus temperature and measured supercooling temperatures [From P.9 of ref. 6]

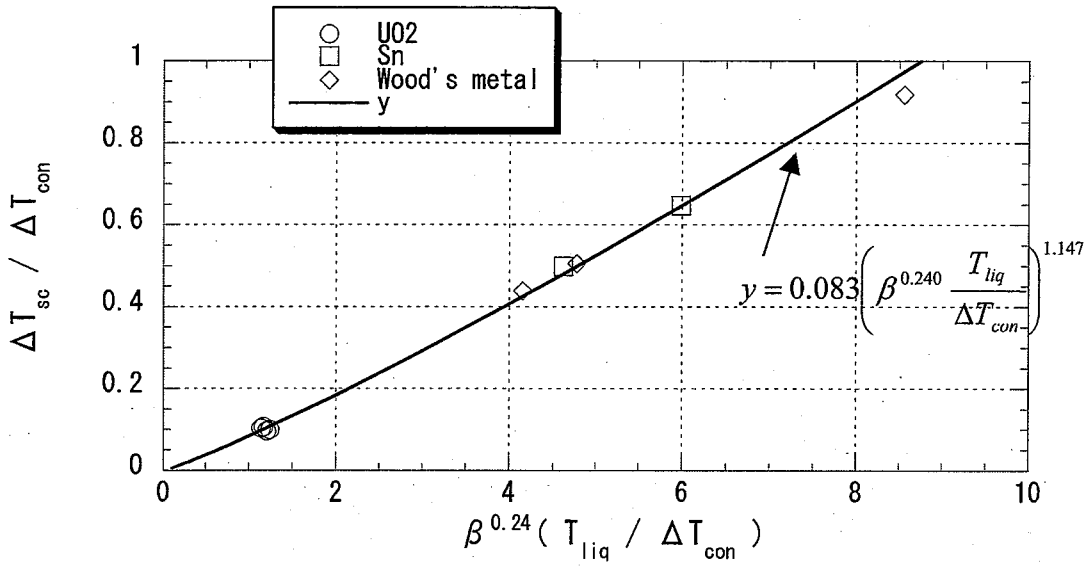

Fig. 3-3 Comparison of experimental data and equation (3-6)

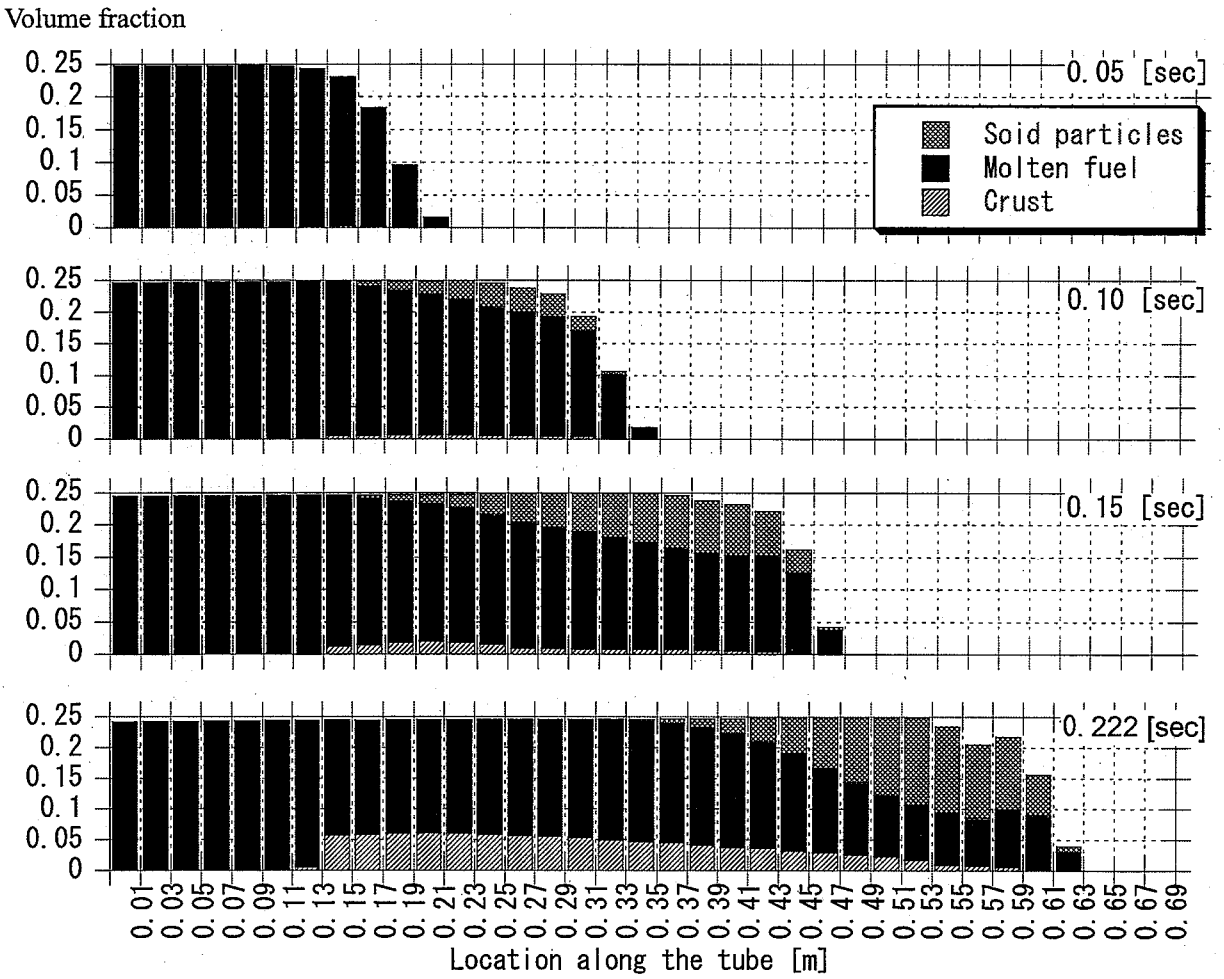

Fig. 3-4 Analysis of Geyser 4 test by SIMMER-III with the newly introduced semi-empirical correlation

4. Conclusion

This study focused attention to the supercooling temperature of molten material in the vicinity of a cold wall, because this temperature controls the energy loss of the flowing molten material.

Results of the present study are summarized as follows:

(1) A semi-empirical correlation to predict supercooling temperature was obtained. In order to increase general applicability of this correlation, various materials with different thermophysical properties and temperature conditions have been evaluated including molten uranium dioxide, tin and wood's metal. This correlation is expressed by temperatures and thermophysical properties both of a molten material and a wall as follows:

$$\Delta T_{sc} = 0.083\beta^{0.275} T_{liq}^{1.147} \left(T_{liq} - \frac{\sqrt{\beta} T_L + T_s}{\sqrt{\beta} + 1} \right)^{-0.147} \quad \text{, where } \beta = \left(\rho c_p \kappa\right)_L / \left(\rho c_p \kappa\right)_w \ .$$

(2) The obtained correlation reasonably reproduced the penetration length of molten stainless steel in comparison with the available experimental data.

Introduction of the obtained correlation into SIMMER-III instead of the input constant variable can improve reliability and accuracy of the freezing model for CDA analysis.

Acknowledgements

I wish to express my gratitude to Mr. D. J Brear, who was International Fellow of Power Reactor and Nuclear Fuel Development Corporation, for his indispensable contribution to basis of this study. I also acknowledge the valuable advice of Mr. Sa. Kondo and Mr. Y. Tobita. This document owes much to experimental study of Dr. Masaki Saito of Tokyo Institute of Technology which was conducted as a joint research program with JNC. My special thanks are due to Mrs. N. Nemura, who belonged in Japan Technical System Co. Ltd., for her significant assistance in SIMMER-III analysis. I am indebted to Mr. M. Sugaya and Mr. T. Kondo of Nuclear Energy System Inc. for their assistance in programming of model and its calculations. I also wish to thank Mr. M. Isozaki for providing me with experimental data in Appendix B. At the end, thanks are due to Dr. Niwa for reading the draft and marking a number of helpful suggestions.

References

1 Y. Tobita, et. al., "An Evaluation on ULOF Event Sequence in the Prototype FBR – An Evaluation of CDA Reflecting the Latest Knowledge-", PNC Report, PNC TN9410 97-097, (September, 1997).

2 Sa. Kondo, et. al., "Status and Achievement of Assessment Program for SIMMER-III, A Multiphase, Multicomponent Code for LMFR Safety Analysis," Proc. 8-th Int. Top. Mtg. on Nuclear Reactor Thermal Hydraulics (NURETH-8), Kyoto, Japan, September 30 – October 4, 1997.

3 Sa. Kondo, et. al., "PHASE 2 CODE ASSESSMENT OF SIMMER-III, A COMPUTER PROGRAM FOR LMFR CORE DISRUPTIVE ACCIDENT ANALYSIS", JNC Report, JNC TN9400 2000-105 (September, 2000).

4 K. Morita, et. al., "SIMMER-III Heat- and Mass-Transfer Model –Model and Method Description-", JNC Report, JNC TN9400 2001-074 (August, 2001).

5 M. Epstein, et. al., "Transient Freezing of a Flowing Ceramic Fuel in a Steel Channel", Nuclear Science and Engineering 61, 310-323(1976).

6 A. Ohno, "The Solidification of Metals", Japanese Text book, Chijin Shokan co., Ltd.

7 W. Kurz and D. J. Fisher, "FUNDAMENTALS OF SOLIDIFICATION", 3rd EDITION, TRANS TECH PUBLICATION (1992).

8 G. Berthoud and B. Duret, "The freezing of molten fuel: reflections and new results", 4th Topical Meeting on Nuclear Reactor Thermal-hydraulics (NURETH-4), Karlsruhe, p. 675 (October 1989).

9 B. C. Pai and H. Jones, " Effect of experimental variables on casting fluidity and fluid life of liquid tin", Material Science and Technology, vol.1, pp398-404, (May 1985).

10 P. Soussan, et. al., "Propagation and Freezing of Molten Material: Interpretation of experimental Results", Proc. International Fast Reactor Safety Meeting, Snowbird, Vol. II, p. 233 (1990).

11 G. Berthoud, "Relocation of molten fuel: determination of the interfacial resistance", Proc. IAEA/IWGFR Technical Committee Meeting on Material Coolant Interactions and Material Movement and Relocation in LMFRs, O-arai, p. 331 (June 1994).

12 D. J. Brear, et. al.,: 1997 Fall mtg. of AESJ, H57(1997).

13 G. Fieg et al, "Freezing phenomena of flowing melts in nonmelting and melting tubes", Proc. Science and Technology of Fast Reactor Safety, Guernsey, Paper 562 (May 1986).

14 T. Hukushige, et., al.,: 1997 Spring Mtg. of AESJ, H51(1997).

15 S. Kobayashi, et. al., 1998 Spring Mtg. of AESJ, I29 (1998)

16 K. Morita, et. al., "SIMMER-III Analytic Equation-of-State Model", JNC Report, JNC TN9400 2000-005 (May, 1999).

17 K. Morita, et. al., "SIMMER-III Analytic Thermophysical Property Model", JNC Report, JNC TN9400 2000-004 (May, 1999).

18 K. Morita, et. al., "Thermodynamic properties and equation of state for fast reactor safety analysis -Part II: Properties of fast reactor materials-", Nuclear Engineering and Design 183 (1998) pp193-211.

Appendix A. Derivation of Bulk Freezing Model

For the superheated molten material, when there is no significant phase change at the interface between the molten material and a cold structure, the following energy balance equation is obtained:

$$\frac{\pi}{4}D_h^2 dz\rho_L C_{pL} dT = \pi D_h dz h_L \left[T_L - \left(T_{liq} - \Delta T_{sc}\right)\right]dt \quad . \tag{A-1}$$

Solving the equation above on temperature and time, the following equation is obtained:

$$\ln\left[T_L - \left(T_{liq} - \Delta T_{sc}\right)\right] = -\frac{4h_L}{\rho_L C_{pL} D_h}t + C \quad . \tag{A-2}$$

When time is zero, the temperature of molten material is $T_L = T_{L0}$, so that the constant, C, is expressed by:

$$C = \ln\left[T_{L0} - \left(T_{liq} - \Delta T_{sc}\right)\right].$$

Therefore, the time when the temperature of molten material becomes T_L can be expressed by:

$$t = \frac{\rho_L C_{pL} D_h}{4h_L}\ln\left[\frac{T_{L0} - \left(T_{liq} - \Delta T_{sc}\right)}{T_L - \left(T_{liq} - \Delta T_{sc}\right)}\right] \quad . \tag{A-3}$$

From this equation, the time t_1 when the molten material is cooled down to its liquidus point is expressed by:

$$t_1 = \frac{\rho_L C_{pL} D_h}{4h_L}\ln\left[1 + \frac{T_{L0} - T_{mp}}{\Delta T_{sc}}\right] \tag{A-4}$$

Next, the equation for energy loss process of the latent heat is obtained after the molten material loses its sensible heat. Here, the molten material stops flowing when it loses a certain portion $(f < 1)$ of latent heat. The time t_2 to satisfy the condition of this flow ceasing is obtained from the following energy balance equation:

$$\frac{\pi}{4}D_h^2 dz\rho_L f L_f = \pi D_h dz h_L \left[T_{mp} - \left(T_{mp} - \Delta T_{sc}\right)\right]t_2, \text{ and} \tag{A-5}$$

$$t_2 = \frac{\rho_L D_h}{4h_L}\frac{fL_f}{\Delta T_{sc}} \tag{A-6}$$

Therefore, the time t_b when the molten material with the initial temperature T_{L0}

forms the blockage is determined from:

$$t_b = t_1 + t_2 = \frac{\rho_L D_h}{4h_L}\left[C_{pL}\ln\left(1+\frac{T_{L0}-T_{mp}}{\Delta T_{sc}}\right)+\frac{fL_f}{\Delta T_{sc}}\right] . \qquad \text{(A-7)}$$

Assuming that the molten material flows at the constant velocity V_L, the penetration length is determined from:

$$L_p = V_L t_b = \frac{\rho_L D_h V_L}{4h_L}\left[C_{pL}\ln\left(1+\frac{T_{L0}-T_{mp}}{\Delta T_{sc}}\right)+\frac{fL_f}{\Delta T_{sc}}\right] . \qquad \text{(A-8)}$$

Appendix B. Stainless Steel Freezing Experiment

B.1. Objective of the Experiment

The original purpose of the stainless steel freezing experiment described here is to evaluate heat loss of molten stainless steel during the transfer from the melting equipment to the test section in which interaction with water is observed. The transfer channel was made of alumina and total length was about 3m. This experiment was performed using MELT-II facility in O-arai Engineering Center, Japan Nuclear Cycle Development Institute.

B.2. Experimental Conditions

Two tests were performed varying the inner diameter of the nozzle. The nozzle was made of alumina, because thermal protection was required for the facility. Schematic diagram of the test section used are shown in Fig. B-1, and the initial test conditions are presented in Table B-1. The stainless steel used in this experiment was SUS-316.

SUS-316 was melted by high-frequency induction heating, and was ejected into the alumina nozzle by gravity force. The initial temperature of the molten stainless steel was measured directly by the tungsten-rhenium thermocouple.

Table B-1 Initial conditions of the stainless steel freezing experiment

Test No.	Initial temperature of molten SUS-316 [deg. C]	Inner diameter of alumina nozzle [mm]	Initial temperature of alumina nozzle [deg. C]
SSFR-30-01	1532	30	See Fig. B-2
SSFR-10-01	1506	10	See Fig. B-2

B.3. Experimental Results

The average velocity of molten stainless steel was obtained by the responses of thermocouples which were installed into the flow area. Figure B-3 shows the relation between the axial position of thermocouples and their response onset time. The average velocity was defined by the slope of plotting point. The penetration length was obtained by dismantling the alumina nozzle after the test.

B.3.1. Results of SSFR-30-10 test

Molten stainless steel did not form a blockage within the alumina nozzle which total length was 2.15m. Based on thermocouple responses, the average velocity of melt was evaluated as 3.965 m/s.

Figure B-4 shows photos of dismantled alumina nozzle after the test. From 0.15 to 0.35m, thin solidified material was observed and its thickness is less than 0.5mm. It was easily detached from the nozzle as shown in the photo. Photos also show that the solidified layer increases its thickness in proportion to the downstream. At the location of 2020mm, the maximum thickness of solidified layer is 5mm, and minimum is 2mm.

B.3.2. Results of SSFR-10-10 test

Dismantling of the alumina nozzle after the test shows that the leading edge of penetrated stainless steel was 1.49m from the inlet. The average velocity of the melt was evaluated 3.45 m/s by responses of thermocouples.

Figure B-5 shows the cross sections of alumina nozzle. One can deduce from these photos that the flow area is filled with the solidified stainless steel. From the location of 1.35m, a gap is observed between the solidified steel and the nozzle, but at the leading edge this gap disappears. (The alumina nozzle was broken during dismantling, but the diameter of solidified steel is equal to the inner diameter of nozzle, so that one can judge that there is no gap.) From the solidified material obtained from 1.35 to 1.49m, it is supposed that the heat loss to the alumina nozzle occurred till the location of 1.35m. Thus, it was concluded that there is uncertainty in the heat loss from 1.35 to 1.49m, so that penetration length was defined as 1.35 - 1.49m.

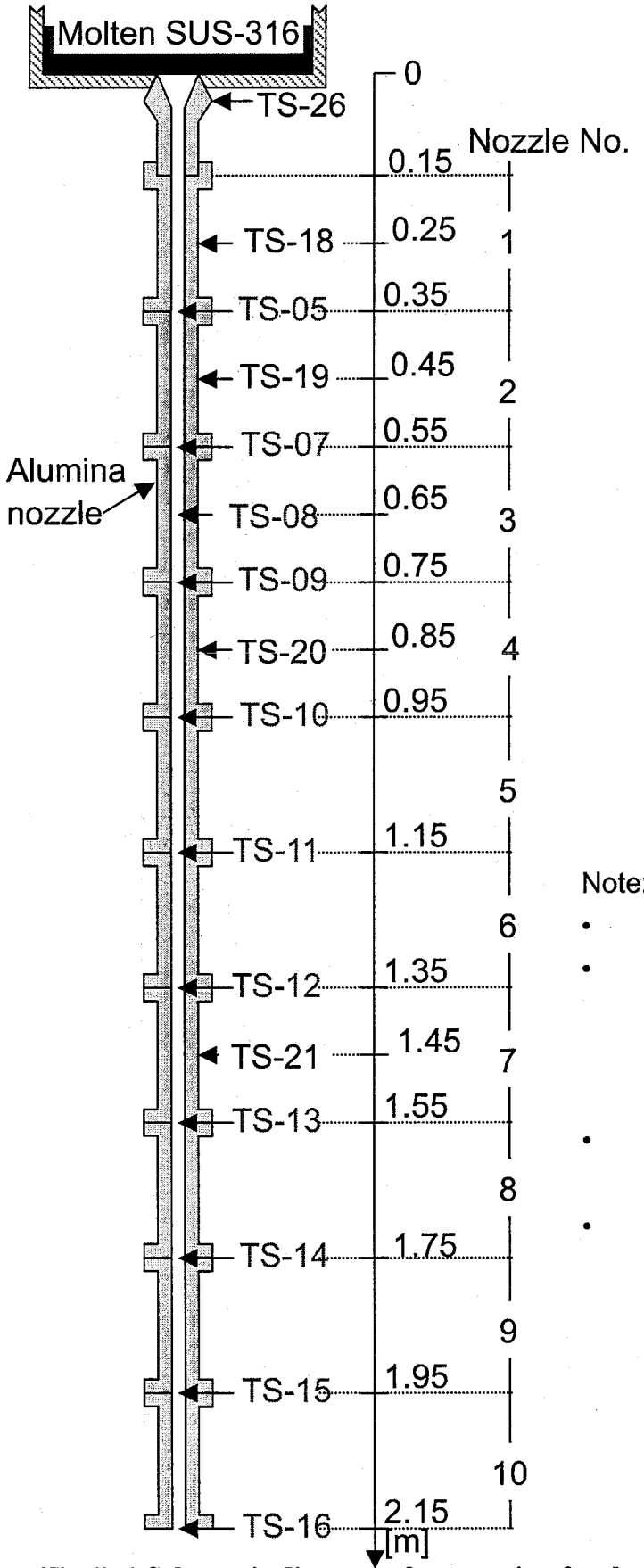

Note:

- TS- means the thermocouple.
- Thermocouples form No.TS-05 to TS16 were installed inside the flow channel to detect arrival of melt.
- TS-08 was installed in SSFR-30-01 test only.
- Thermocouples form No.TS-18 to TS21 and TS-26 were installed outside the flow channel to measure wall temperature.

Fig. B-1 Schematic diagram of test section for the stainless steel freezing experiment

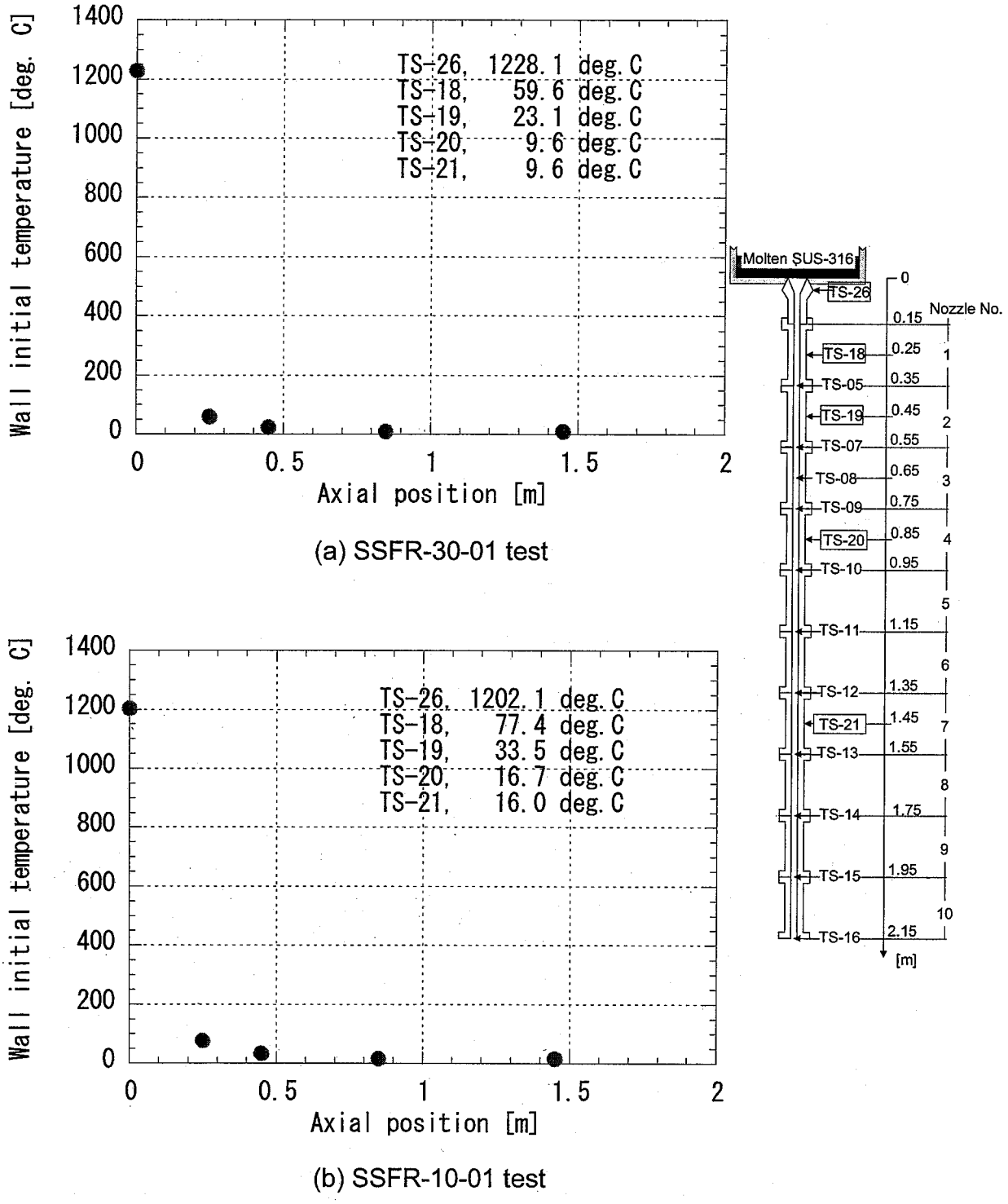

Fig. B-2 Initial temperature distribution of alumina nozzle

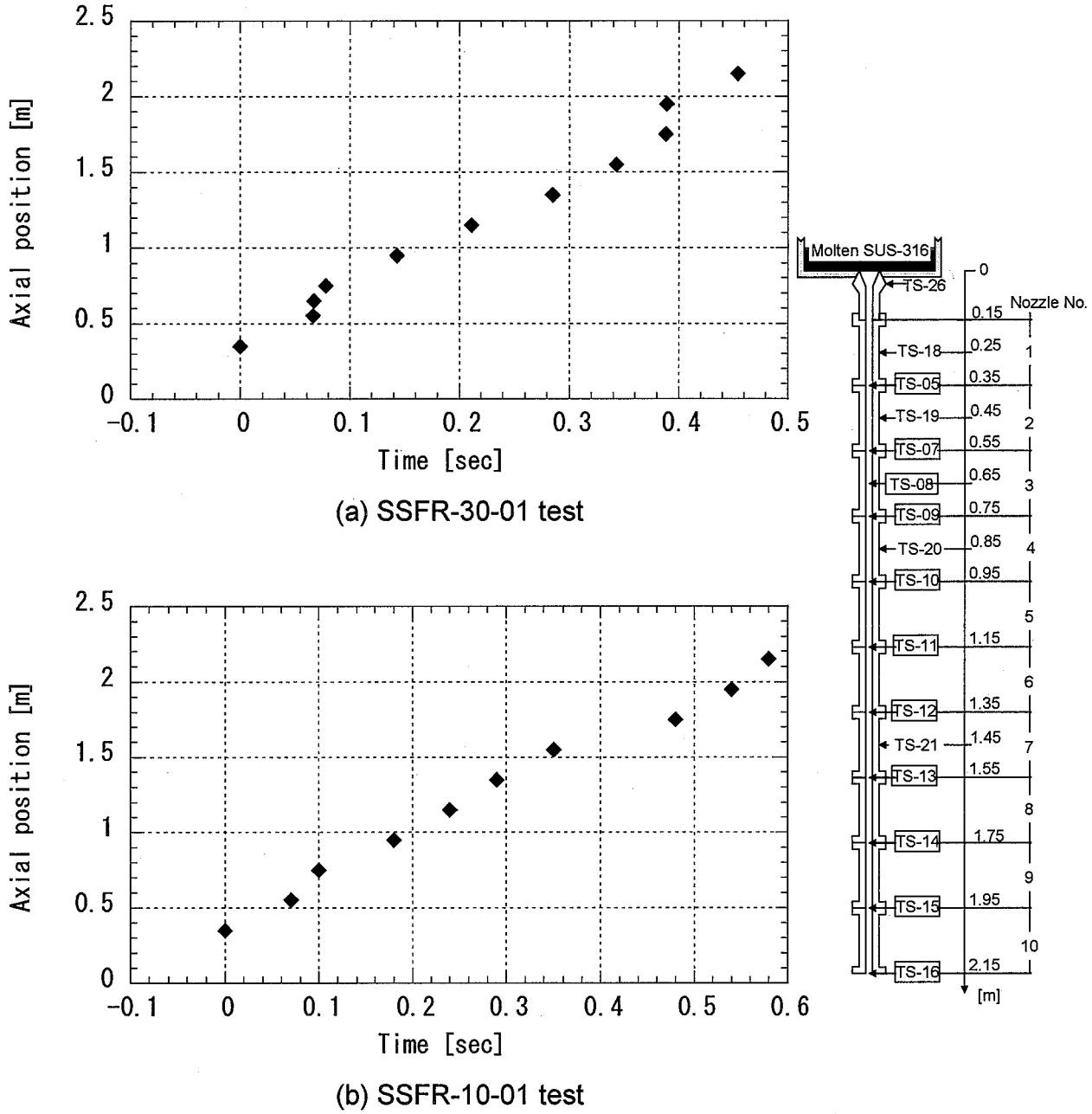

Note: Response onset of TS-05 is set time zero.

Fig. B-3 Times of thermocouple responses onset

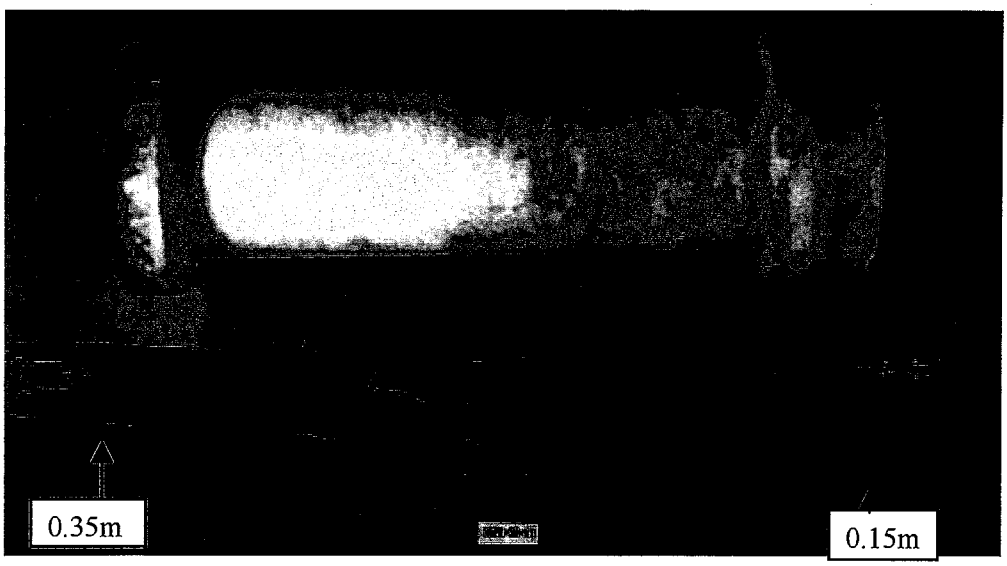

Solidified fragments extracted form nozzle No.1 (0.15~0.35m)

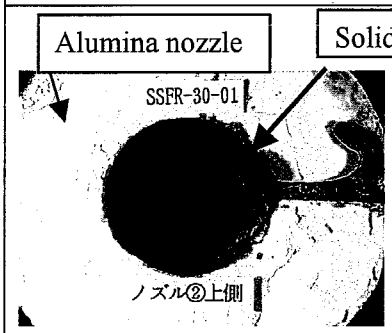

Cross section at 0.35m

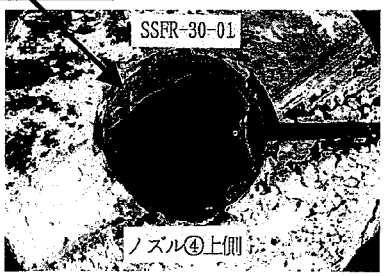

Cross section at 0.75m

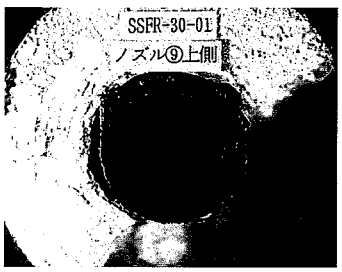

Cross section at 1.75m

Cross section at 1.95m

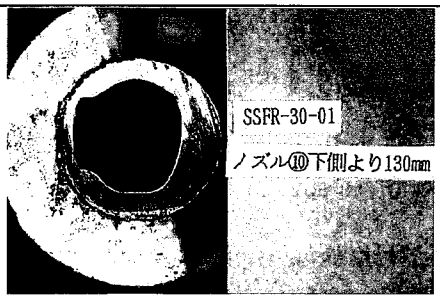

Cross section at 2.02m

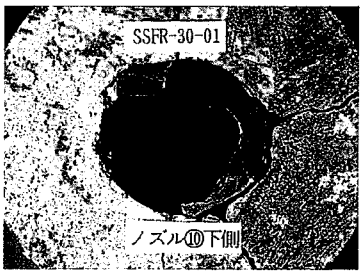

Cross section at 2.15m

Fig. B-4 Photos of dismantled alumina nozzle after SSFR-30-01test

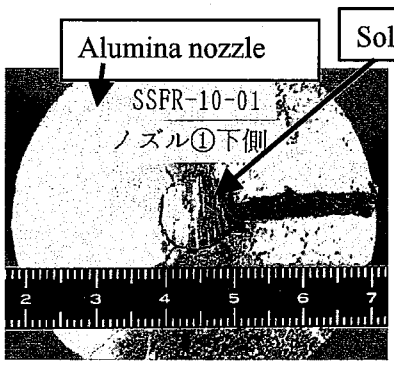

Cross section at 0.35m

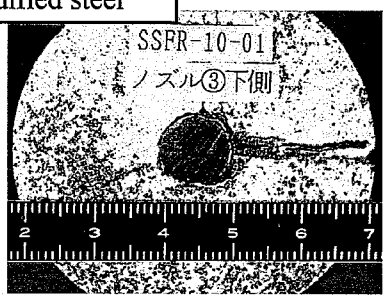

Cross section at 0.75m

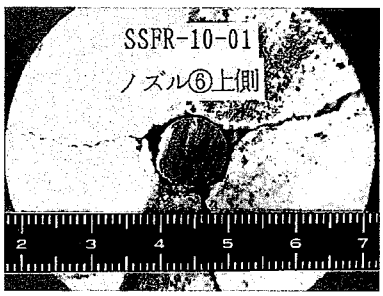

Cross section at 1.15m

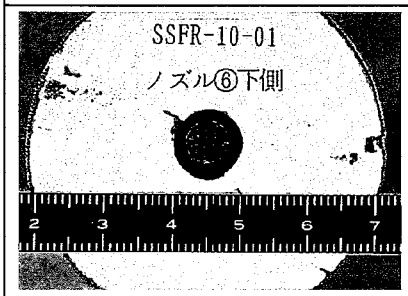

Cross section at 1.35m

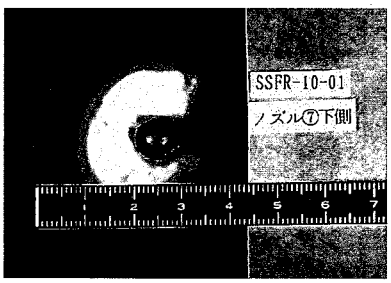

Bottom view of nozzle no. 7 (at 1.49m)

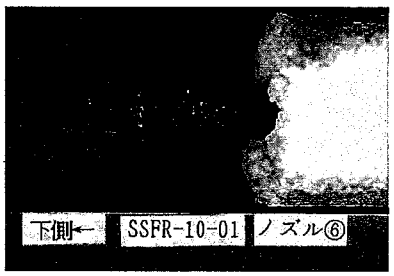

Side view around 1.35m

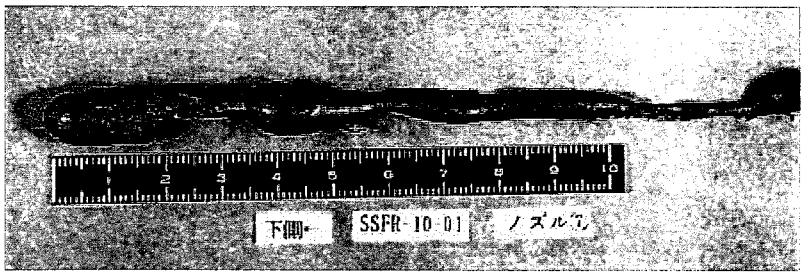

Fragment of solidified SUS-316, 1.49m(left)・ 1.35m・ right・

Fig. B-5 Photos of dismantled alumina nozzle after SSFR-10-01test